Available online at www.sciencedirect.com
SCIENCE DIRECT
NDT&E International 39 (2006) 562–568
NDT&E international
www.elsevier.com/locate/ndteint

Eddy current measurements of electrical conductivity and magnetic permeability of porous metals

X. Ma[a,*], A.J. Peyton[a], Y.Y. Zhao[b]

[a]School of Electrical and Electronic Engineering, University of Manchester, Manchester M60 1QD, UK
[b]Department of Engineering, University of Liverpool, L69 3GH, UK

Received 17 January 2006; received in revised form 22 March 2006; accepted 29 March 2006
Available online 5 June 2006

Abstract

This paper presents a method, which simultaneously estimates the electrical conductivity and magnetic permeability of porous metals. Porous Cu and Fe manufactured by the lost carbonate sintering process have been tested. An air-cored solenoid coil was designed for the measurements of rod-shaped samples when inserted coaxially with the coil. It was theoretically found that the phase-frequency response of the normalised eddy current signal of the coil is virtually independent of the radius, electrical conductivity and magnetic permeability of the test samples. For non-magnetic, conductive porous Cu, the electrical conductivity was measured with a calibration curve of the coil relating the impedance change and the electrical conductivity of the sample. For magnetic porous Fe, the imaginary part of the signal at the lowest frequencies can be used to estimate the permeability. The measured conductivity values of the porous Cu are shown in the paper in comparison with that of bulk materials with known conductivity. The measured permeability values of the porous Fe are given and the sample-length effect on the measurements is also discussed.

Keywords: Eddy currents; Conductivity; Permeability; Impedance; Porous metals

1. Introduction

Porous metals or metal foams have recently attracted considerable attention in both academia and industry due to their exceptional mechanical, thermal, acoustic, electrical and chemical properties. Close-cell foams are mainly developed for structural applications such as energy absorption, where most important considerations are relative density or porosity, specific strength and ductility in compression. Open-cell foams are manufactured for functional applications such as sound absorption, heat dissipation and catalyst support. The lost carbonate sintering (LCS) process [1] is a versatile method for manufacturing porous metals with fine and open cells. LCS consists of mixing a metal and a carbonate (K_2CO_3) in powder form, compacting and sintering of the powder mixture followed by carbonate removal. Compared to the sintering-dissolution process (SDP) previously introduced [2], the LCS method is able to eliminate the space-holder carbonate particles more rapidly and more thoroughly. It is particularly suitable for metals with higher melting points, such as Cu- and Fe-based alloys.

Recently, eddy current methods have been used for the measurement of electrical properties of aluminium foams [3,4]. The relative density, or porosity, and the microstructure of the foams significantly affect the induced eddy currents in the test samples and hence change the coil impedance due to the amount of metal within the foam and the tortuosity of the current path. By measuring this impedance change, the nature of the material may be inferred by correlating the coil impedance using analytical and/or experimental approaches to the characteristic quantities of interest such as conductivity and permeability.

In our previous work [4], a double air-cored solenoid sensor was designed for the measurements of electrical conductivity of the rod-shaped samples (one coil for excitation and another for detection). Both experimental measurements and finite element simulations have shown that the phase signature of the sensor output is approximately

*Corresponding author. Tel.: +44 161 3064808; fax: +44 161 3064789.
E-mail address: Xiandong.Ma@manchester.ac.uk (X. Ma).

0963-8695/$ - see front matter © 2006 Elsevier Ltd. All rights reserved.
doi:10.1016/j.ndteint.2006.03.008

test-sample independent for a given sensor/material geometry. The bulk measurement data were therefore used to calibrate the phase signature response to evaluate the unknown conductivity of aluminium foams.

This paper presents the latest development of the eddy current method, which is used to simultaneously estimate the electrical conductivity and magnetic permeability of porous Cu and Fe samples manufactured by the LCS method. Measurement results of these samples are also presented in the paper.

2. Theory

Let us consider the problem, as shown in Fig. 1. The axis of a single layer solenoid coil of radius b, n turns and width l is assumed to coincide with the z-axis with the centre of the coil at the origin of a cylindrical coordinate system (r, θ, z). A rod-shaped metal sample of radius a, electrical conductivity σ and magnetic permeability μ is placed coaxially with the solenoid coil. For the sinusoidal waveform excitation cases with complex phasor notation, the Maxwell equations can be finally derived to a differential equation for the magnetic vector potential A_θ component due to the circular symmetry of the problem:

$$\frac{\partial^2 A_\theta}{\partial r^2}+\frac{1}{r}\frac{\partial A_\theta}{\partial r}-\frac{A_\theta}{r^2}-j\omega\mu\sigma A_\theta=0 \tag{1}$$

where ω is the applied angular frequency, $\mu=\mu_r\mu_0$, μ_0 is the permeability of free space i.e., $4\pi\times10^{-7}\,H/m$, μ_r is the relative permeability.

Naturally, the solution of vector potential $\mathbf{A}_\theta$ must account for all the relevant boundary conditions specific to the particular application. Having obtained the vector potential $\mathbf{A}_\theta$, the electric field strength $\mathbf{E}$ (V/m) is known through a gauge choice, which makes $\mathbf{E}=\partial\mathbf{A}/\partial t$. The induced voltage in the coil is thus computed by taking the line integral of the vector $\mathbf{E}$ around the coil loop. This final complex voltage represents the coil impedance because the magnitude of the excitation current is normally known.

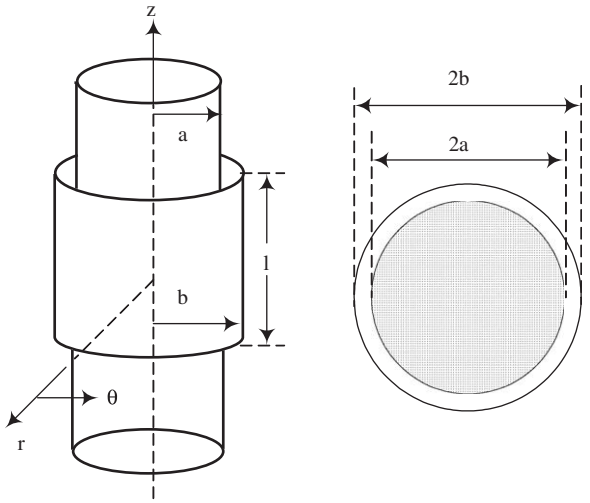

Fig. 1. Schematic diagram of solenoid coil and rod-shaped test sample.

Libby [5] has reported an analytical solution for the vector potential and the induced voltage when a unit current passes through a single-turn coil encircling an infinitely long cylindrical test sample within it. Neglecting the impedance of the coil itself, the coil impedance is given by

$$Z=\omega\mu_r\mu_0\pi a^2\left[\frac{2}{ka}\left(\frac{\mathrm{ber}'(\mathrm{ka})+j\mathrm{bei}'(\mathrm{ka})}{\mathrm{ber}(\mathrm{ka})+j\mathrm{bei}(\mathrm{ka})}\right)\right]+j\omega\mu_0\pi(b^2-a^2), \tag{2}$$

where ka is referred to as the reference number ($\mathrm{ka}=a\sqrt{\omega\mu_r\mu_0\sigma}$), ber and bei are the real and imaginary parts of Bessel function of the first kind, respectively, and ber′ and bei′ are their first derivatives [6].

If Z_0 is assumed as the empty coil impedance in the absence of a test sample, then $Z_0=j\omega\mu_0\pi b^2$ by letting $a=0$. For a coil of n turns and width l, the magnitude of all the coil impedance should be multiplied by a coefficient that equals to n^2/l.

The value of Z_n is defined by $Z/|Z_0|$ and further given by

$$Z_n=\mu_r\eta\left[\frac{2}{\mathrm{ka}}\left(\frac{\mathrm{ber}'(\mathrm{ka})+j\mathrm{bei}'(\mathrm{ka})}{\mathrm{ber}(\mathrm{ka})+j\mathrm{bei}(\mathrm{ka})}\right)\right]+j(1-\eta). \tag{3}$$

Thus, the real and imaginary parts of Z_n are, respectively

$$R_n=\frac{2\mu_r\eta}{\mathrm{ka}}\frac{\mathrm{ber}(\mathrm{ka})\mathrm{ber}'(\mathrm{ka})+\mathrm{bei}(\mathrm{ka})\mathrm{bei}'(\mathrm{ka})}{\mathrm{ber}(\mathrm{ka})^2+\mathrm{bei}(\mathrm{ka})^2}, \tag{4}$$

$$X_n=\frac{2\mu_r\eta}{\mathrm{ka}}\frac{\mathrm{ber}(\mathrm{ka})\mathrm{bei}'(\mathrm{ka})-\mathrm{bei}(\mathrm{ka})\mathrm{ber}'(\mathrm{ka})}{\mathrm{ber}(\mathrm{ka})^2+\mathrm{bei}(\mathrm{ka})^2}+1-\eta, \tag{5}$$

where $\eta=a^2/b^2$, and is called the fill-factor.

Consider two extreme cases of $\omega=0$ and $\omega=\infty$. When $\omega=0$, there is

$$X_{n|\omega=0}=1+(\mu_r-1)\eta. \tag{6}$$

This means that for a non-magnetic conductive sample ($\mu_r=1$) there is no impedance change caused and the magnetic flux penetrates the specimen as in the free space under dc condition. However, for a magnetic and conductive sample ($\mu_r>1$), the impedance change caused is dominated by its relative permeability μ_r under dc condition for a given coil/material geometry.

When $\omega=\infty$, it can be derived

$$X_{n|\omega=\infty}=1-\eta. \tag{7}$$

This implies that magnetic flux is totally linked with the test material under condition of $\omega=\infty$.

As an example, the values of R_n and X_n calculated by Eqs. (4) and (5) are shown in Fig. 2 when the coil radius b is 12.5 mm for four test samples as given in Table 1. Here, magnetic and non-magnetic materials display different electromagnetic effects. Non-magnetic conductive objects oppose the penetration of the applied magnetic field into the target due to the skin effect, thus resulting in a net reduction in the coil reactance. In contrast, magnetic

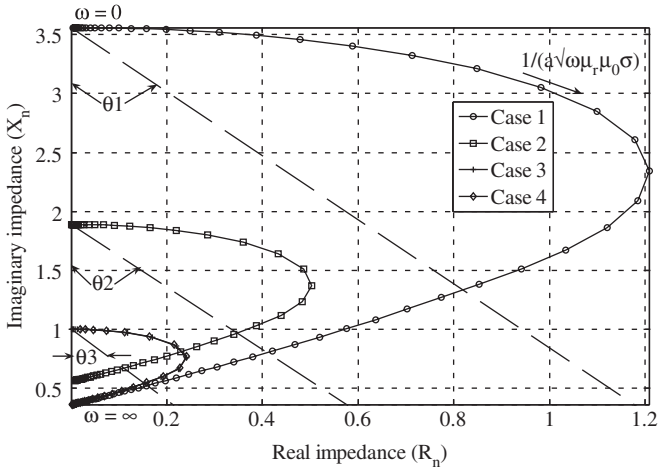

Fig. 2. Normalised impedance curves of the test samples.

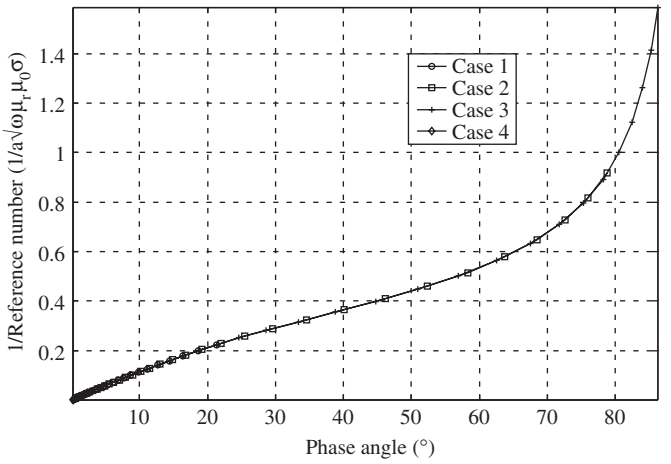

Fig. 3. Relationship between phase angle and reference number, showing that phase angle is virtually test material independent.

Table 1
Test samples used for the display of normalised impedance curves, where μ_r: relative permeability, σ: electrical conductivity (MS/m), a: sample radius (mm) and η: fill-factor

	μ_r	σ	a	η
Case 1	5	2	10.0	0.64
Case 2	3	0.2	8.33	0.44
Case 3	1	0.2	10.0	0.64
Case 4	1	20	10.0	0.64

objects cause the magnetic flux to flow preferentially through the target, resulting in an increased coil reactance.

Apparently, the overall magnitude of the signal is highly dependent on the radius, conductivity and permeability of the specimens. Therefore, the phase angle of the eddy current signal is more interesting to analyse. As shown in Fig. 2, the phase angle θ is mathematically defined by

$$\theta = \tan^{-1}\left(\frac{R_n}{X_{n|\omega=0} - X_n}\right). \tag{8}$$

Substituting Eqs. (4) and (5) into Eq. (8), the phase angle θ then becomes

$$\theta = \tan^{-1}\left(\frac{\mathrm{ber(ka)ber'(ka)} + \mathrm{bei(ka)bei'(ka)}}{\mathrm{ka}/2(\mathrm{ber(ka)}^2 + \mathrm{bei(ka)}^2) - \mathrm{ber(ka)bei'(ka)} + \mathrm{bei(ka)ber'(ka)}}\right). \tag{9}$$

With this formula, the phase angle of four curves shown in Fig. 2 is then calculated and displayed in Fig. 3. This indicates that a non-linear relationship exists between phase angle and the reference number, irrespective of the test sample's radius, conductivity and permeability under analysis. Furthermore, Fig. 2 also shows that their imaginary parts virtually remain constant at lower reference numbers, i.e., at the lower frequencies, from which the permeability of materials can be estimated from Eq. (6) when ω is supposed to approach to 0.

3. Experiments

Experiments were carried out to estimate the conductivity and permeability of porous metals by means of the phase signature invariance of the test materials for a given coil geometry. In the experiments, a solenoid coil of radius $b = 12.5$ mm, width $l = 11$ mm, and $n = 32$ turns was used. Porous Cu and Fe samples manufactured by the LCS method at Liverpool University were used as the test samples. These samples were machined into a rod shape with a diameter of around 20 mm and a height of around 32 mm and are characterised mainly by their relative density and pore size. Four sets of porous Cu samples were tested with pore sizes of 250–500 μm, 500–710 μm, 710–1000 μm and larger than 1000 μm, respectively, each having four different relative densities of 0.15, 0.2, 0.25 and 0.3. Six porous Fe samples were used, one with a pore size of 425–710 μm and a relative density of 0.25, four samples with a pore size of 710–1000 μm and relative densities ranging from 0.24–0.36, and one with a pore size of 1000–1500 μm and a relative density of 0.25.

A Solartron SL 1260 impedance analyser was used in the tests, which can supply a sinusoidal signal with variable frequencies outputted to the coil in a frequency-scanning manner. The induced voltage in the coil was measured by the voltage input channel of the analyser. The analyser then recorded the ratios of the induced voltage across the coil and the current flowing through the coil, obtaining the real

and imaginary parts of the coil impedance. During the tests, the analyser was programmed to provide 50 frequencies on a logarithmic scale ranging from 1 Hz to 1 MHz. The impedance values measured when a sample was present inside the coil were normalised with the measurement values when the coil was empty. This would eliminate the effects of the background coupling and determine the relative magnitude of eddy current signal with regards to the background measurements.

The operation frequency f is significant in that it determines the penetration of magnetic field below the test sample surface, which is described by skin depth $\delta = 1/\sqrt{\pi f \mu_r \mu_0 \sigma}$. Depending on the sample parameters, an effective frequency range should be selected. Supposing a rod-shaped porous sample of pore size c, radius a, conductivity σ and permeability μ, the lower frequency f_{low} and higher frequency f_{high} are then given by, respectively

$$f_{low} = \frac{1}{\pi \mu_r \mu_0 \sigma a^2}, \tag{10}$$

$$f_{high} = \frac{1}{\pi \mu_r \mu_0 \sigma c^2}. \tag{11}$$

When $f_{low} \leqslant f \leqslant f_{high}$, the electromagnetic skin depth is ensured from an initial depth of pore size to a depth comparable to the sample's radius, thus resulting in the measurements to be made with a relatively good accuracy.

As is known from the previous section, Eq. (6) is derived from Eq. (5) when $\omega = 0$ is applied. Thus, it could be understood that the relative permeability μ_r can be estimated using Eq. (6) from the measurements at the lowest frequencies. By integrating each measurement over a long time, e.g. 10 s, at low frequencies, SL 1260 impedance analyser was able to acquire the measurement data with an acceptable sensitivity at lower frequencies in the order of 10 Hz. Frequencies lower than 10 Hz resulted in extremely low sensitivity measurements due to the inductive nature of the sensor.

4. Measurement results

4.1. Non-magnetic porous Cu

For non-magnetic conductive porous metals, their electrical conductivity σ can be estimated through [4]

$$\sigma = \frac{1}{\omega \mu_r \mu_0 (aX(\theta))^2}, \tag{12}$$

where $\mu_r = 1$, and the pre-calculated values of $X(\theta)$ can be calibrated using the complex impedance of bulk materials with known conductivity, such as aluminium.

Fig. 4 shows the impedance curves of the porous Cu samples and the 99.99% pure aluminium with $\sigma = 37.67$ MS/m at frequencies ranging from 100 Hz to 158 kHz. The variation of the overall magnitude of the signals is due to the variations in the diameter among the samples although they all have a nominal diameter of 20 mm. Values of the inverse ka of the bulk aluminium are plotted against phase angle θ in Fig. 5, and the relationship between them is then fitted numerically with a polynomial expression

$$X(\theta) = 1.41 \times 10^{-4} + 0.0081\theta + 7.76 \times 10^{-6}\theta^2 - 1.80 \times 10^{-6}\theta^3 + 2.23 \times 10^{-8}\theta^4. \tag{13}$$

The theoretically calculated curve as shown in Fig. 3 is also included in Fig. 5 in order to compare these two curves. It is found that both curves match closely. Eq. (13) is therefore used as the calibration curve to evaluate the electrical properties of the porous samples.

Fig. 6 shows the measured conductivity corresponding to the set of the porous Cu samples with pore sizes of 250–500 μm. By taking a mean value within the selected frequency range, the values of equivalent conductivity of the porous Cu samples are deduced. With the same

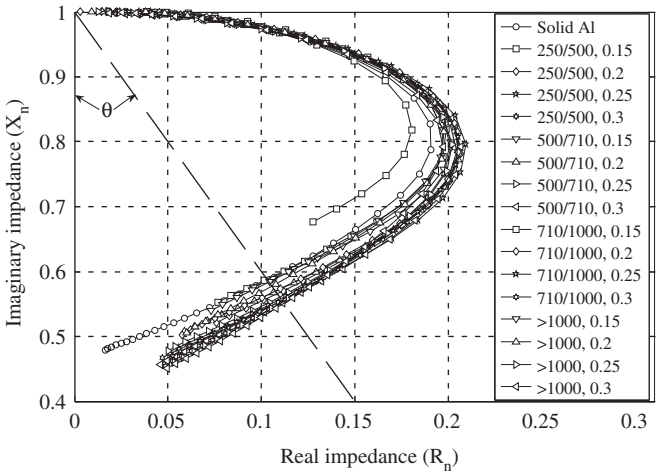

Fig. 4. Normalised impedance curves of the porous Cu samples and solid aluminium at frequencies in a range of 100 Hz–158 KHz.

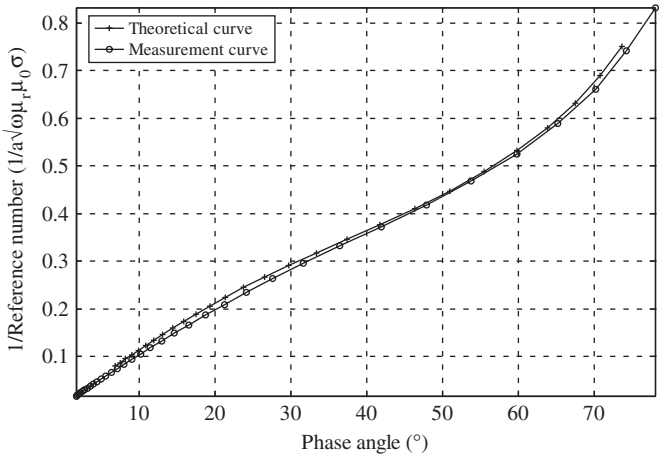

Fig. 5. Reference number versus phase angle for bulk aluminium, where the theoretical curve is also shown.

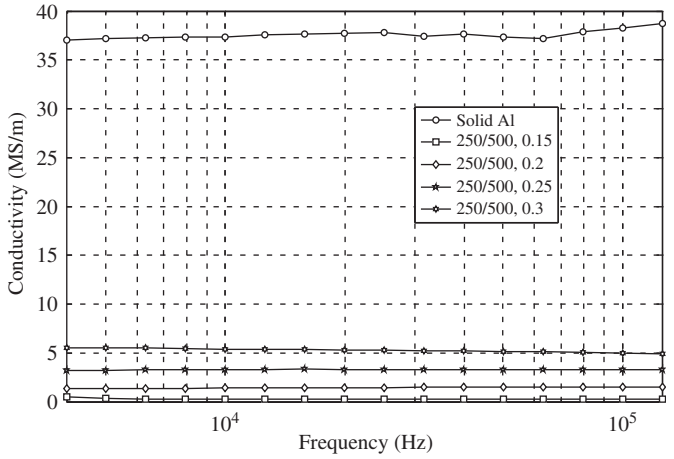

Fig. 6. Measured conductivity of the porous Cu samples with pore sizes of 250–500 μm but different relative densities of 0.15, 0.2, 0.25 and 0.3 at a frequency range of 3.98–126 kHz.

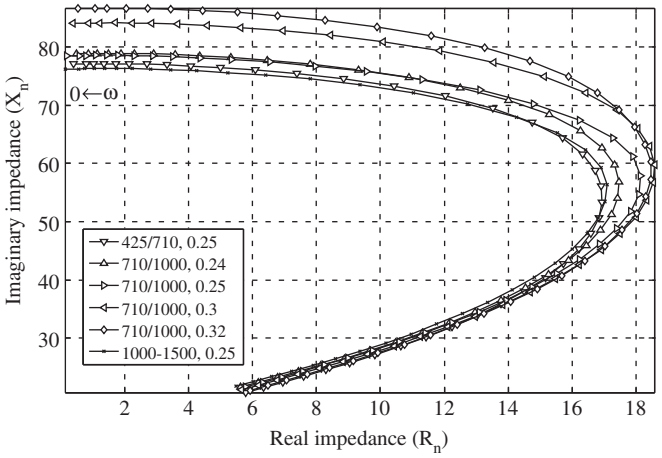

Fig. 7. Normalised impedance curves of the six porous Fe samples at frequencies in a range of 63 Hz–500 KHz.

Table 2
Measured electrical conductivity (MS/m) of the porous Cu samples

Relative density (pore size)	0.15	0.2	0.25	0.3
250–500 μm	0.255	1.437	3.289	5.268
500–710 μm	0.843	2.501	4.474	6.258
710–1000 μm	1.227	2.914	4.627	5.896
>1000 μm	1.545	3.074	4.724	5.506

method, three other sets of the porous Cu samples with pore sizes of 500–710 μm, 710–1000 μm and larger than 1000 μm are also measured, as given in Table 2. As can be seen from the results, for the samples with similar pore sizes, lower relative density leads to lower conductivity because of the lower Cu volume ratio in the samples. For the samples with the same relative density, larger pore sizes are normally associated with a better-bonded network structure of cell walls. Consequently, this results in a higher electrical conductivity compared to that of the samples with smaller pore sizes. However, when the relative density reaches to 0.3, the effect of pore size on the porous samples' conductivity becomes insignificant. The measured conductivity of bulk aluminium is 38.357 MS/m, compared to its actual value of $\sigma = 37.67$ MS/m. Thus, the measurement errors with this method could be within 2.0%.

4.2. Magnetic porous Fe

Fig. 7 shows the measured impedance curves of the six porous Fe samples at frequencies ranging from 63 Hz to 500 kHz. As can be seen from these curves, their imaginary parts virtually remain constant at lower frequencies. With Eq. (6), the relative permeability μ_r of the samples can be derived from X_n components at lower frequencies, which is shown in Fig. 8. The values of μ_r become stable when the applied operation frequency is decreased to below 500 Hz.

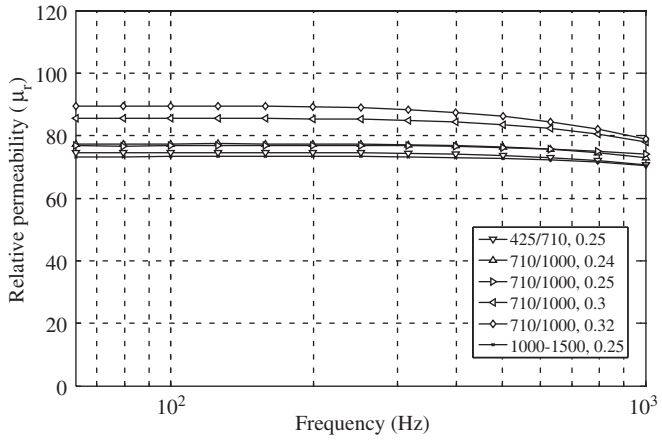

Fig. 8. Values of relative permeability μ_r of the six porous Fe samples at lower operation frequencies of 63 Hz–1 kHz.

Table 3
Measured electrical conductivity σ and relative permeability μ_r of the porous Fe samples

Test samples (pore size, rel. density)	Electrical conductivity (MS/m)	Relative permeability μ_r	Values of μ_r (after compensation)
425–710 μm, 0.25	0.994	74.585	175.275
710–1000 μm, 0.24	0.953	77.420	181.936
710–1000 μm, 0.25	1.039	76.755	180.374
710–1000 μm, 0.3	1.354	85.472	200.856
710–1000 μm, 0.32	1.457	89.507	210.341
1000–1500 μm, 0.25	0.952	73.248	172.132
Solid aluminium	38.180		

The values of μ_r of the porous Fe samples are given in Table 3 at the lowest operation frequency of 63 Hz.

Having obtained the parameter μ_r, the electrical conductivity σ of the porous Fe samples can then be evaluated through Eq. (12) in the same way as in dealing with the

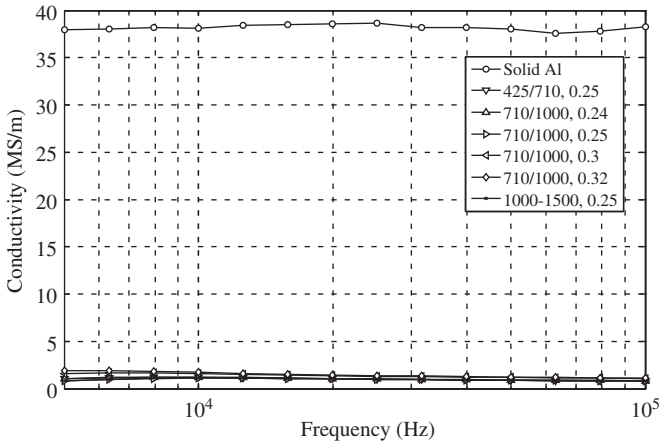

Fig. 9. Measured conductivity of the six porous Fe samples at the frequencies in a range of 3.98–126 kHz.

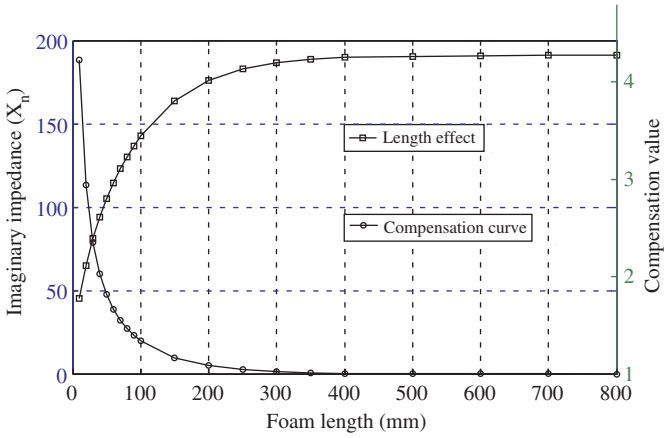

Fig. 10. The effect of ferrite-based samples with different lengths on the imaginary impedance X_n at a frequency of 63 Hz, where the compensation curve for final μ_r determination is also shown.

porous Cu samples. Eq. (13) is still used as the calibration curve to evaluate the values of σ of the porous Fe samples. Fig. 9 shows the measured conductivity corresponding to the six porous Fe samples. The values of σ of the samples are also given in Table 3 by taking a mean value within the selected frequency range. For the four porous Fe samples with pore sizes of 710–1000 μm but with relative densities ranging from 0.24 to 0.32, one can see that a lower relative density leads to a reduction in both conductivity σ and permeability μ_r because of a lower Fe volume ratio in the samples. However, the difference between the values of μ_r and σ is not significant, because the porous Fe samples under tests have similar relative densities.

4.3. Finite-length effect

It is necessary to investigate the effect of the finite length of a sample on the complex impedance of a solenoid coil as the theoretical solutions described in Section 2 assumes an infinitely long rod-shaped sample. The sensor geometry given in Fig. 1 was simulated using Maxwell (Ansoft Corporation), which was a 3D finite element package and offered a piecewise solution to field problems by splitting the problem into a series of small tetrahedral elements over which the field values are approximated. A problem region was solved of 5 times the size of the sensor model to ensure that the applied boundary conditions did not over constrain the solution. The surrounding air was assigned by the material property of a vacuum. A total of 67,673 tetrahedral elements were meshed to ensure that the simulations converged to 0.5% target error.

Solid aluminium samples of radius $b = 10.0$ mm were simulated at two lengths of 30 mm and 300 mm in a same frequency range of 100 Hz–158 KHz as used in Fig. 4. It was found that the impedance curves of the two aluminium samples match very well; this confirms that the problem of the finite length does not occur for the non-magnetic conductive porous Cu samples.

As for the magnetic and conductive materials, ferrite-based alloy bars of radius $b = 10.0$ mm, conductivity $\sigma = 2.1$ MS/m and relative permeability $\mu_r = 1000$ were simulated at 20 lengths from 10 mm to 800 mm, i.e., at lengths of 10, 20, 30, 40, 50, 60, 70, 80, 90, 100, 150, 200, 250, 300, 350, 400, 500, 600, 700 and 800 mm, respectively. The complex impedances of the coil due to the presence of the ferrite bars present inside the coil were computed at $f = 63$ Hz, the lowest operation frequency as used in Fig. 7, and are shown in Fig. 10. Apparently the value of X_n component is sample-length dependent; however, it reaches stable when the ferrite bar is longer than 350 mm. If a sample length of 800 mm is assumed long enough concerning a coil width of 11 mm, a compensation curve is then derived for the test samples with different short lengths, which is also shown in Fig. 10. For a test sample of length 30 mm, the compensation coefficient is around 2.35. With this coefficient, the permeability μ_r of the porous Fe samples is now compensated and shown in Table 3 correspondingly.

5. Conclusions

This study has shown that eddy current techniques can be effectively used to examine both electrical conductivity and magnetic permeability of porous Cu and Fe samples. Theoretical analysis shows that the phase-frequency response of the normalised eddy current signal of a solenoid coil is virtually independent of the radius, electrical conductivity and magnetic permeability of the test samples. For non-magnetic conductive porous Cu samples, their electrical conductivity is measured with a calibration curve of the coil relating the impedance change and the electrical conductivity of the sample with a known conductivity. For magnetic porous Fe samples, the signal shows its imaginary part remains relatively constant at lower frequencies, from which the permeability of the samples is approximately estimated. Appropriate selection

of an effective operation frequency range is critical in achieving reliable results, which depends largely on the coil configuration and the parameters of the porous metal samples, such as the pore size and radius of the samples. For the permeability evaluation of the porous Fe samples, the measurement results were dependent largely on the data at low frequencies, which demanded that the impedance analyser be able to acquire the data with an acceptable sensitivity at these frequencies.

The measurement results demonstrate that the electrical properties of porous metals are strongly dependent on both porosity and its macrostructure (pore size). For the porous Fe samples, a lower relative density leads to a reduction in both conductivity σ and permeability μ_r because of a lower Fe volume ratio in the samples. Further work should include forward problem solutions of a solenoid coil when a finite-length rod-shaped sample is present coaxially in the coil using a finite element simulation method. By fully considering the combination effect of finite-length, electrical properties (electrical conductivity and magnetic permeability) and the operation frequency on the coil impedance, it is hoped this work will assist in the development of a solution capable of estimating more accurately the conductivity and permeability.

Acknowledgements

The authors would like to thank Mr. T. Fung, Mr. S.J. Wang and Dr. L.P. Zhang for the contributions in the sample preparations and UK Engineering and Physical Sciences Research Council (EPSRC) for the financial support of the project.

References

[1] Zhao YY, Fung T, Zhang LP, Zhang FL. Lost carbonate sintering process for manufacturing metal foams. Scripta Mater 2005;52:295–8.
[2] Zhao YY, Sun DX. A novel sintering-dissolution process for manufacturing Al foams. Scripta Mater 2001;44:105–10.
[3] Dharmasena KP, Wadley HNG. Eddy current characterization of metal foams. In: Proceedings of Materials Research Society spring symposium, San Francisco. 13–15 April 1998, p. 171–6.
[4] Ma X, Peyton AJ, Zhao YY. Measurement of the electrical conductivity of open-celled aluminium foam using non-contact eddy current techniques. NDT & E Int 2005;38:359–67.
[5] Libby HL. Introduction to electromagnetic nondestructive test methods. New York: Wiley; 1971.
[6] McLachlan NW. Bessel functions for engineers. Oxford: Clarendon Press; 1955.